ELSEVIER

Journal of Power Sources 76 (1998) 167–174

JOURNAL OF POWER SOURCES

Thermodynamic studies of cobalt and cadmium additions to nickel hydroxide as material for positive electrodes

Ken-ichi Watanabe [a,*], Naoaki Kumagai [b]

[a] *Shin-Kobe Electric Machinery, No. 8-7, 2-Chome, Nihonbashi-Honcho, Chuo-ku, Tokyo 103, Japan*
[b] *Department of Applied Chemistry and Molecular Science, Faculty of Engineering, Iwate University, Morioka 020, Japan*

Received 16 June 1998; accepted 23 August 1998

Abstract

Nickel oxide is used as the positive electrode in nickel–cadmium and nickel–metal-hydride batteries. The physical and the electrochemical effects due to the addition of cobalt and cadmium to nickel hydroxide powders are investigated. X-ray diffraction analysis shows that the d_{001} value (interlayer distance in the nickel hydroxide) decreases with increase in cobalt content, while the d_{100} value increases with increase in cadmium content. The open-circuit potential in discharge follows an S-shaped curve in 3 M KOH electrolyte. The results are discussed with respect to thermodynamic theory. The experimentally obtained OCP variation is in good agreement with calculated data using thermodynamic theory with one fitting parameter, ϕ/RT; ϕ is an interaction energy parameter (J mol^{-1}) and RT is the product of the gas constant and absolute temperature. The ϕ/RT and E^0 (standard electrode potential) values are found to decrease with increase in cobalt content, while the addition of cadmium has little effect on the ϕ/RT and E^0 values. A difference between the OCP data and the calculated value occurs at the end of discharge; this difference tends to increase with increase in cobalt content.

Keywords: Thermodynamic studies; Cobalt; Cadmium; Nickel hydroxide; Positive electrodes

1. Introduction

A significant amount of work has been published on the thermodynamic properties of insertion electrodes, such as proton insertion electrodes [1–8] and lithium insertion electrodes [9–14]. According to thermodynamic theory, the equilibrium potential E of an insertion electrode can be separated into three terms [3,11,13]: a standard electrode potential E^0, an interaction term $\epsilon_{\text{int}}(x)$, and an entropy contribution term, i.e.,

$$E = E^0 + \epsilon_{\text{int}}(x) + \psi \times (RT/F) \times \ln((1-x)x) \qquad (1)$$

where both the interaction term and the entropy contribution term are functions only of x (insertion degree). In this paper, attention is focused on the interaction term ($\epsilon_{\text{int}}(x)$).

It is widely accepted that the nickel oxide electrode works as an insertion electrode for protons [15–19], i.e.,

$$\text{NiOOH} + \text{H}^+ + \text{e}^- \Leftrightarrow \text{Ni(OH)}_2 \qquad (2)$$

The variation in open-circuit potential (OCP) of the nickel oxide electrode using thermodynamic considerations has been reported by Barnard et al. [6,7]. It was found that during charge, the OCP varies between the nickel oxidation states of 2 and 2.25; nevertheless, the OCP remains constant for nickel oxidation states higher than 2.25. This suggests that the oxidation reaction is a one-phase system between the nickel oxidation states of 2 and 2.25, while for other nickel oxidation states, the reaction is a two-phase system.

In previous work [8], however, we have revealed that the OCP of the nickel oxide electrode followed an S-shaped curve over a wide reduction range in 3 M KOH electrolyte; this result indicates that the reduction is a one-phase system. In contrast, for the nickel oxide electrode in 3 M LiOH, a two-step OCP curve is clearly observed. In the first stage, the OCP curves are S-shaped, while in the second stage, the OCP curves are L-shaped. The second

* Corresponding author. Tel.: +81-3-5695-6126; Fax: +81-3-5695-6141

0378-7753/98/$19.00
PII: S0378-7753(98)00150-5

stage indicates that the reaction is a two-phase system. Moreover, the variation in OCP depends on the crystallite size of the β-nickel hydroxide (β-$Ni(OH)_2$). This evidence shows that carefully controlled experiments are required to clarify the behaviour of the nickel oxide electrode.

It has been widely reported that co-precipitation of cobalt hydroxide on the nickel hydroxide improves the utilization at high temperature and provides a longer life [15,18,20–25]. On the other hand, co-precipitation of cadmium hydroxide has been used to inhibit electrode swelling [15,18,23].

In this study, the physical and thermodynamic considerations are studied in order to gain a better understanding of why improvement of the nickel oxide electrode occurs when cobalt and cadmium hydroxide are co-precipitated with nickel hydroxide during the deposition process. The results are obtained using a paste-type nickel oxide electrode [25–29], with spherical nickel hydroxide powder and a foamed nickel substrate, immersed in 3 M KOH electrolyte.

2. Thermodynamic theory

In order to describe the variation in the OCP of the nickel oxide electrode as a function of the reduction process, thermodynamic theory is used. The charge–discharge reaction, Eq. (2), can be translated into Eq. (3) or Eq. (4), in which $0 < x < 1$, namely:

$$NiOOH + H^+ + e^- \Leftrightarrow Ni(OH)_2 \quad (2)$$

$$NiOOH + xH^+ + xe^- \Leftrightarrow H\,x\,NiOOH\ (0 < x < 1) \quad (3)$$

$$NiOOH + xH^+ + xe^- \Leftrightarrow (Ni(OH)_2)\,x(NiOOH)1 - xe \times (0 < x < 1) \quad (4)$$

The value of x denotes the mole fraction of $Ni(OH)_2$ in the nickel oxide electrode in Eq. (4). Strictly speaking, however, this assumption is not true, as indicated by Atlung and Jacobsen [4], because the nickel oxide electrode is assumed to be an insertion electrode. Therefore, the products of the electrode reaction are distributed over the entire volume of the nickel oxide active material.

The thermodynamic theory of metal oxide insertion electrodes has been described by many authors [1–14]. To the best of our knowledge, the first such study was reported by Crandall et al. [3]. In the work reported here, the equation modified by Barnard et al. [6,7] is used. The equation is slightly modified in terms of its symbols [8].

$$E = E^0 + (RT/F)(\phi/RT)(2x - 1) + \psi(RT/F)\ln((1 - x)/x). \quad (5)$$

where E is the electrode potential at constant pH (V); E^0 is the standard electrode potential (V); R is the gas constant (J K^{-1} mol^{-1}); T is the absolute temperature (K); F is the Faraday constant (C); x is the mole fraction of $Ni(OH)_2$ in the nickel oxide; ϕ is the interaction energy parameter (J mol^{-1}). The second term (interaction term) is linear with respect to x. In Eq. (5), all higher-power interaction terms in x may be neglected [3]. It should be emphasized that Eq. (5) is only true if the nickel oxide electrode reaction is symmetrical, as indicated by Barnard et al. [6,7].

According to Crandall et al. [3], ψ is the proton–electron spatial correlation coefficient and takes a value of 2 ($\psi = 2$) if the electron and proton are not closely correlated, or a value of 1 ($\psi = 1$) if they are spatially correlated. In our previous paper [8], however, the value of 1 ($\psi = 1$) is more closely fitted to the experimental data than that of the value of 2 ($\psi = 2$) in 3 M KOH and 3 M NaOH electrolytes. Therefore, we have used the value of 1 ($\psi = 1$), i.e.,

$$E = E^0 + (RT/F)(\phi/RT)(2x - 1) + 1(RT/F)\ln((1 - x)/x). \quad (6)$$

This relationship shows that $E = E^0$ at $x = 0.5$ (145.5 mAh per g of active material discharge in Eq. (1)). In this paper, the $E - x$ relationship of the nickel oxide electrode is observed in 3 M KOH and compared with the curve calculated from Eq. (6).

3. Experimental

3.1. Preparation of electrode materials and nickel electrode

Nickel foam (2 cm × 2 cm, 96% porosity, Sumitomo Electric Industries) was used as the nickel electrode substrate. The following eight types of β-type nickel hydroxide (β-$Ni(OH)_2$) powders were used as the positive electrode materials. Samples A and F are from Nihon Kagaku Sangyo; samples B to E, G, and H are from Tanaka Chemical. These nickel hydroxide samples with different cobalt and cadmium contents were obtained by adding alkaline solution to mixed Ni^{2+}, Co^{2+} and Cd^{2+} solutions.

Cobalt metal powder (N.V. Union Miniere) was added at 5 wt.% to the hydroxide powders to increase and stabilize the utilization of the active materials [26,27]. Hydroxypropyl–Methyl–Cellulose (HPMC) (Shin-Etsu Chemical) and a polytetrafluoroethylene (PTFE) dispersion (Daikin Industries) were used as binders.

The preparation of the nickel electrode has been described previously [25]. The geometrical surface area of the nickel electrode was 4 cm^2 and the electrode loading of the nickel hydroxide was about 0.14 g cm^{-2}. These nickel electrodes were spot-welded with a 6-mm nickel ribbon which served as a current-collector.

Table 1
Physical properties of nickel hydroxide samples

Sample	Chemical composition			Mean diameter (μm)	BET surface area ($m^2\ g^{-1}$)
	Ni (wt.%)	Co (wt.%)	Cd (wt.%)		
A	61.9	0.19	≪0.01	14	38
B	58.8	2.5	≪0.01	12	27
C	57.0	4.6	≪0.01	14	22
D	51.5	9.9	≪0.01	11	30
E	58.7	0.62	3.1	12	24
F	56.5	0.73	6.4	11	19
G	53.9	5.4	3.2	16	20
H	47.9	10.2	3.2	13	30

3.2. Analysis of nickel hydroxide powder and electrochemical measurement of nickel electrode

The apparatus for the analysis of the physical properties of the nickel hydroxide powder was the same as that used previously [25], i.e., a RINT-1100 diffractometer (Rigaku) using Cu K_α radiation with a nickel filter at 40 kV and 20 mA.

A three-compartment glass beaker cell was used for the electrochemical measurements. A nickel mesh was mounted as the counter electrode, and 3 M KOH served as the electrolyte. This solution was prepared from reagent grade chemicals and distilled water. The potential was measured against a Hg/HgO (3 M KOH) reference electrode in the same solution. The electrolysis cell was placed in an incubator held at 20°C. The electrochemical behaviour of various samples (A–H) was first characterized by constant-current charge–discharge measurements.

Charging was performed at a rate of 7.0 mA cm^{-2} for 6 h. The charging capacity was about 120% of the theoretical capacity of the nickel hydroxide positive electrode. Discharging was then carried out at a rate of 7.0 mA cm^{-2} down to 0.1 V vs. Hg/HgO, followed by recharge at a rate of 7.0 mA cm^{-2} for 6 h. The theoretical capacity of the nickel hydroxide is 289 mAh per g of active material by assuming the following electrode reaction:

$$NiOOH + H^+ + e^- \Leftrightarrow Ni(OH)_2 \qquad (2)$$

Intermittent discharges were then carried out at a rate of about 7.0 mA cm^{-2} for 30 min (30 mAh per g of active material discharge) down to 0.1 V vs. Hg/HgO. To reach a quasi-equilibrium OCP after intermittent discharge, a period of 20 to 60 h at a constant temperature was required in order to obtain a uniform distribution of H^+-ions throughout the working electrode. The intermittent discharge was followed by a period for about 45–60 h on open-circuit, or until the OCP changed less than 0.2 mV h^{-1} at a constant temperature.

4. Results and discussion

4.1. Physical properties of nickel hydroxide samples

The chemical compositions and physical properties of the nickel hydroxide samples (A–H) are presented in Table 1. The cobalt and the cadmium contents are different in each sample. The mean diameter of these samples is in

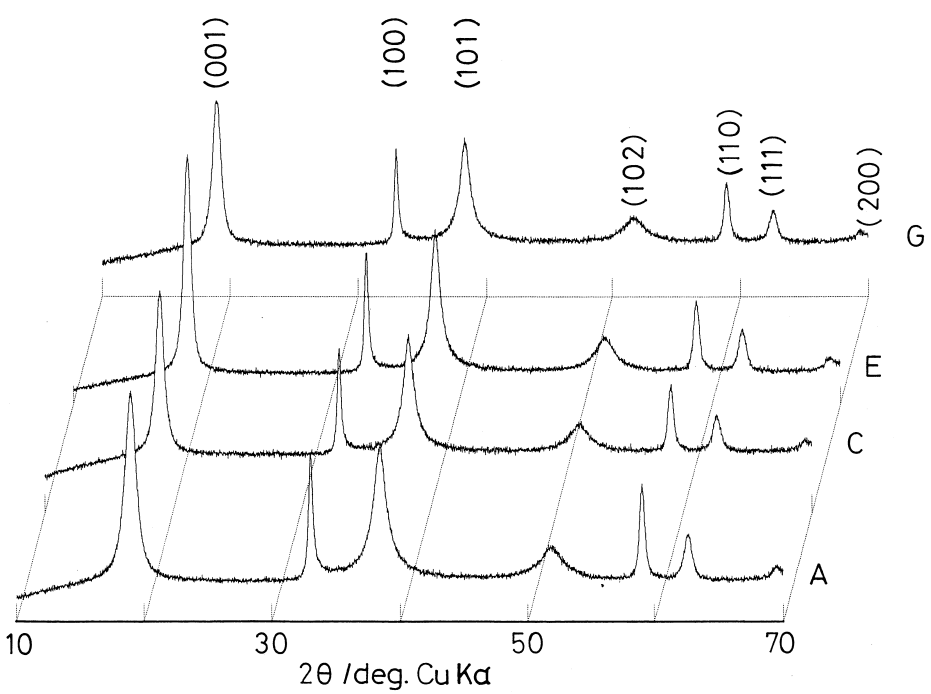

Fig. 1. XRD patterns of samples showing the Miller indices of β-$Ni(OH)_2$ samples: A: 0.19 wt.% Co, Ref. [8]; C: 4.6 wt.% Co; E: 0.62 wt.% Co, 3.1 wt.% Cd; G: 5.4 wt.% Co, 3.2 wt.% Cd.

Table 2
FWHM, *d*-values, and peak intensity in (001), (100) and (101) diffraction lines of nickel hydroxide samples

Sample	(001)			(100)			(101)		
	$FWHM_{001}$ (degrees)	d_{001} (nm)	Peak intensity (count s^{-1})	$FWHM_{100}$ (degrees)	d_{100} (nm)	Peak intensity (count s^{-1})	$FWHM_{101}$ (degrees)	d_{101} (nm)	Peak intensity (count s^{-1})
A	1.095	0.4682	5604	0.450	0.2709	3642	1.153	0.2342	3828
B	0.935	0.4667	5024	0.411	0.2709	3249	0.931	0.2341	3834
C	0.815	0.4657	4979	0.415	0.2709	3016	0.985	0.2342	3351
D	0.841	0.4633	3910	0.430	0.2703	2405	0.872	0.2336	2986
E	0.730	0.4682	6370	0.349	0.2717	3534	0.874	0.2346	3820
F	0.745	0.4677	6490	0.357	0.2722	3512	0.903	0.2352	3983
G	0.806	0.4657	4336	0.363	0.2715	2679	0.942	0.2343	2883
H	0.860	0.4643	3074	0.395	0.2712	2018	0.855	0.2346	3207

the range 11 to 16 μm, and the BET surface area is between 19 and 38 $m^2\ g^{-1}$.

Typical X-ray diffraction (XRD) patterns of the samples (A, C, E, and G) are presented in Fig. 1. These samples have different cobalt and cadmium contents and give almost the same XRD pattern due to the β-type nickel hydroxide (β-$Ni(OH)_2$) with a brucite-type structure and a hexagonal unit cell. Peaks for the cobalt and the cadmium components are not observed. This indicates that the two components are incorporated into the crystal lattice of the β-$Ni(OH)_2$. The full width of the half-maximum intensity (FWHM), the *d* values, and the peak intensity of the respective samples in the (001), (100), and (101) diffraction lines are listed in Table 2. The FWHMs tend to decrease with increase in cobalt and cadmium contents. This suggests that the crystallite size of the nickel hydroxide powder tends to increase with increase in the cobalt and the cadmium contents [30]. The d_{001} values (*c* value, which indicates the interlayer distance of a brucite-type structure) decrease with increase in the cobalt content, as reported in Ref. [25]. On the other hand, the d_{100} values (*a* value = $(2/\sqrt{3})d_{100}$, *a* value corresponds to the Ni–Ni distance within the layers) increase with increase in the cadmium content as shown in Fig. 2.

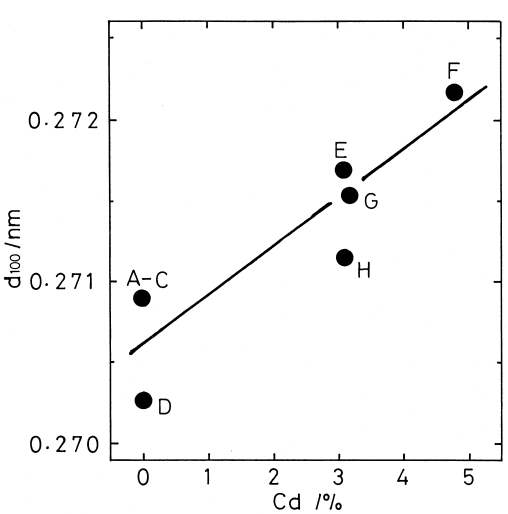

Fig. 2. Effect of cadmium content on d_{100} value. A: 0.19 wt.% Co; B: 2.5 wt.% Co; C: 4.6 wt.% Co; D: 9.9 wt.% Co; E: 0.62 wt.% Co, 3.1 wt.% Cd; F: 0.73 wt.% Co, 6.4 wt.% Cd; G: 5.4 wt.% Co, 3.2 wt.% Cd; H: 10.2 wt.% Co, 3.2 wt.% Cd.

4.2. Constant-current charge–discharge curves

The charge–discharge and subsequent charge curves of samples A to E, G, and H are given in Figs. 3–5. Because samples E and F display nearly the same charge–discharge curve, we have used the data of sample E as typical data. Note that the potential range (*y*-axis) in Fig. 3 to Figs. 4 and 5 differ.

For the initial charge curves (Fig. 3), a small hump always appears during the early stage of charge (in the charge capacity range about 0 to 100 mAh per g of $Ni(OH)_2$). The potential of sample E is higher than that of sample A, while that of samples B, C, D, G, and H is much lower than that of sample A in the charge capacity range 100 to ~300 mAh per g of $Ni(OH)_2$. As mentioned earlier in Fig. 2, the d_{100} values increase with increase in the cadmium content. The large d_{100} values would decrease the electronic conductivity [18] of the nickel oxide and thus result in a higher polarization in sample E. On the other hand, the addition of cobalt (samples B to D, G, and H) produces a lower polarization.

The initial discharge curves (Fig. 4) show that the potential decreases continuously. Furthermore, the potential of samples A and E is higher than that of samples B to D, G, and H; this result indicates that the addition of cobalt decreases the discharge potential as reported by many other authors [15,18,24,25].

For the second charge curves (Fig. 5), however, the potential variation is greater than that for the initial charge curves (Fig. 3). For example, the nickel oxide electrode potentials in the second charge curves are lower than those of the initial charge curves in the charge capacity range 0 to ~200 mAh per g of $Ni(OH)_2$. On the other hand, in the charge capacity region above ~200 mAh per g of $Ni(OH)_2$, the potentials of the second charge curves are higher than those of the initial charge curves.

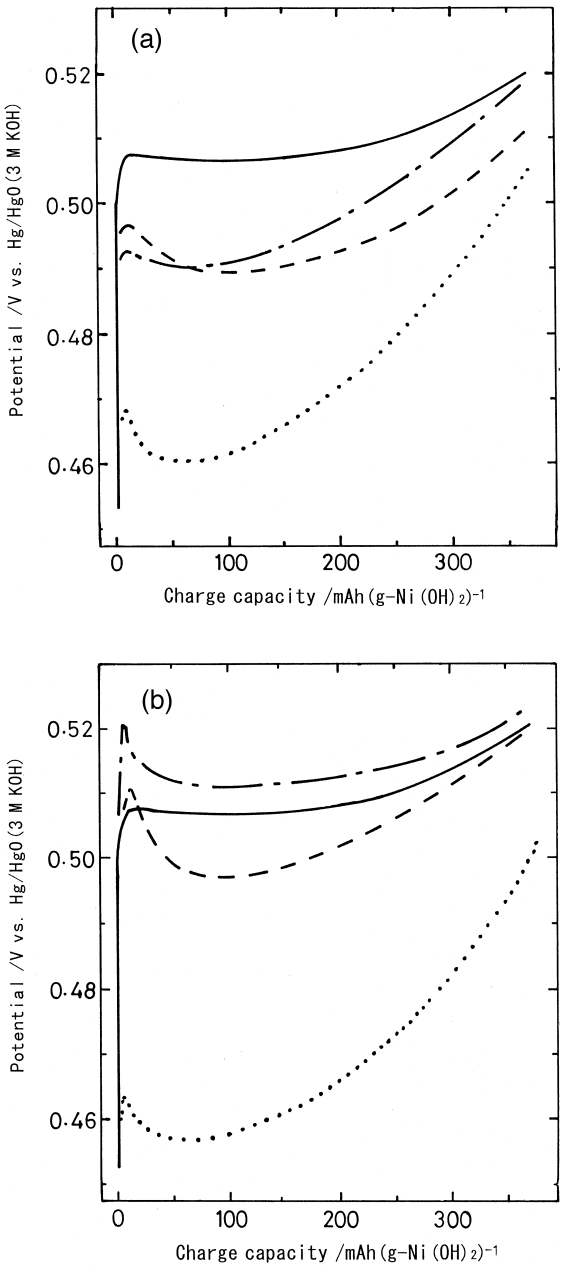

Fig. 3. Initial charge curves of samples at a charge rate of 7.0 mA cm^{-2}. (a) (initial charge curves), (————) A: 0.19 wt.% Co, Ref. [8]; (— · —) B: 2.5 wt.% Co; (---) C: 4.6 wt.% Co; (· · ·) D: 9.9 wt.% Co. (b) (initial charge curves), (————) A: 0.19 wt.% Co; (— · —) E: 0.62 wt.% Co, 3.1 wt.% Cd; (---) G: 5.4 wt.% Co, 3.2 wt.% Cd; (· · ·) H: 10.2 wt.% Co, 3.2 wt.% Cd.

The potential variation is greater in samples B to D than that in sample A, See Fig. 5(a). For instance, the potential of samples B to D is lower than that of sample A in the charge capacity range 0 to ~200 mAh per g of $Ni(OH)_2$, while samples B to D show higher potential values than that of sample A in the charge capacity region above ~200 mAh per g of $Ni(OH)_2$.

The potential variation is greater in samples G and H than in sample E, see Fig. 5(b). The second charge curves of samples A and E are, however, virtually identical. These data show that the addition of cobalt decreases the charge potential as reported by many other authors [15,18,24,25].

In the charge capacity region above ~300 mAh per g of $Ni(OH)_2$, an obvious charge plateau appears (Fig. 5). This is caused by the oxygen-evolution reaction [15]:

$$2OH^- \Rightarrow (1/2)0_2 \uparrow + H_2O + 2e^- \quad (7)$$

Four cycled continuous-current charge–discharge measurements were made for each electrode. It was found that

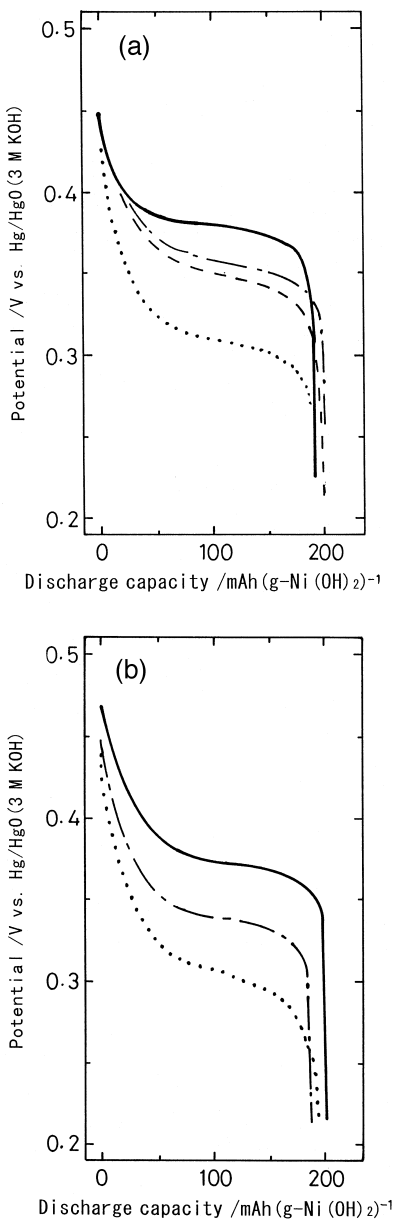

Fig. 4. Initial discharge curves of samples at a discharge rate of 7.0 mA cm^{-2}. (a) (initial discharge curves), (————) A: 0.19 wt.% Co, Ref. [8]; (— · —) B: 2.5 wt.% Co; (---) C: 4.6 wt.% Co; (· · ·) D: 9.9 wt.% Co. (b) (initial discharge curves), (————) E: 0.62 wt.% Co, 3.1 wt.% Cd; (— · —) G: 5.4 wt.% Co, 3.2 wt.% Cd; (· · ·) H: 10.2 wt.% Co, 3.2 wt.% Cd.

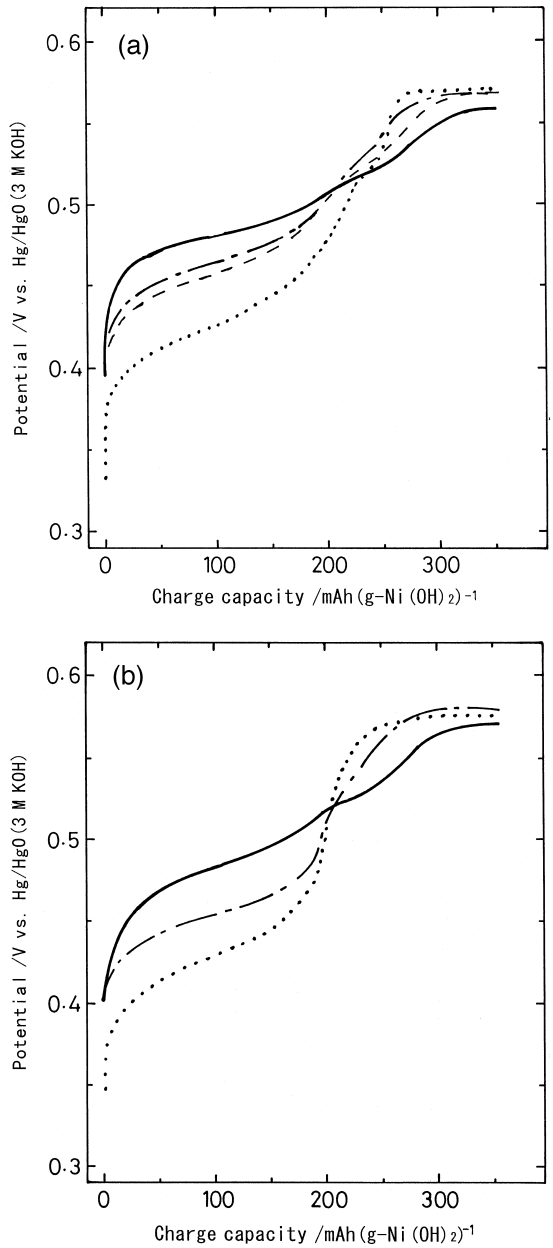

Fig. 5. Second charge curves of samples at a charge rate of 7.0 mA cm^{-2}. (a) (second charge curves), (————) A: 0.19 wt.% Co, Ref. [8]; (— · —) B: 2.5 wt.% Co; (---) C: 4.6 wt.% Co; (· · ·) D: 9.9 wt.% Co. (b) (second charge curves), (————) E: 0.62 wt.% Co, 3.1 wt.% Cd; (— · —) G: 5.4 wt.% Co, 3.2 wt.% Cd; (· · ·) H: 10.2 wt.% Co, 3.2 wt.% Cd.

there was little change in the charge–discharge curves after the second cycle. These data show that once the oxidation and the reduction occurred, the electrochemical properties of nickel oxide electrode changed significantly.

4.3. Intermittent current discharge curves

Intermittent current discharge was carried out for the second discharge, and the OCP variations was measured. The OCP curves (character and solid line) and the calculated curves (broken line) of samples A to E, G, and H are presented in Fig. 6 as a function of discharge capacity. Because samples E and F gave nearly the same OCP curves, the data of sample E was used as a typical curve. The charged state of the nickel oxide is assumed to be

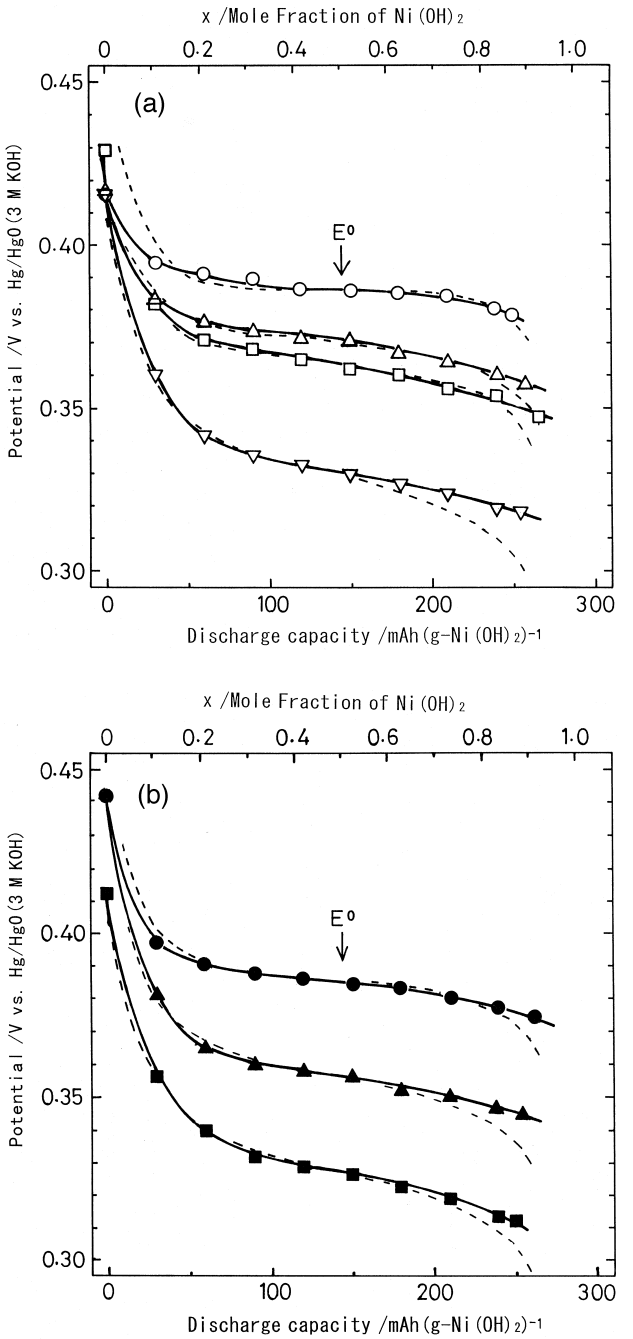

Fig. 6. Comparison of OCP versus discharge state in samples. (a) A: (○) Experimental OCP, ---: Calculated ($\phi/RT = 2.0$), 0.19 wt.% Co, Ref. [8] B: (△) Experimental OCP, ---: Calculated ($\phi/RT = 1.8$), 2.5 wt.% Co, C: (□) Experimental OCP, ---: Calculated ($\phi/RT = 1.7$), 4.6 wt.% Co, D: (▽) Experimental OCP, ---: Calculated ($\phi/RT = 1.3$), 9.9 wt.% Co. (b) E: (●) Experimental OCP, ---: Calculated ($\phi/RT = 1.9$), 0.62 wt.% Co, 3.1 wt.% Cd, G: (▲) Experimental OCP, ---: Calculated ($\phi/RT = 1.5$), 5.4 wt.% Co, 3.2 wt.% Cd, H: (■) Experimental OCP, ---: Calculated ($\phi/RT = 1.3$), 10.2 wt.% Co, 3.2 wt.% Cd.

$x = 0$ in Eq. (4). The value of x in the discharge is calculated from the mass of the nickel hydroxide, the value of the current, and the discharge time.

In these OCP curves, samples A and E exhibit higher values than the other samples. Moreover, the OCP slopes are steeper in proportion with the cobalt content. These data clearly indicate that the addition of cobalt affects the variation in OCP during reduction.

In order to quantify the OCP variation in Fig. 6, thermodynamic considerations have been used. The E^0 values in Eq. (6) were experimentally obtained, assuming that the E^0 values were the OCP at $x = 0.5$ (145.5 mAh per g of active material discharged in Fig. 6). A least-square error fit of Eq. (6) was made with just one fitting parameter ϕ/RT to the experimentally measured OCP data. The resulting E^0 and ϕ/RT values for these samples are shown in Table 3. The fit of the experimental data to the calculated broken line in Fig. 6 is good except at the end of discharge. Moreover, both the OCP data and the calculated line display an S-shaped curve. We conclude, therefore, that the discharge reaction of these nickel oxide electrodes in 3 M KOH electrolyte indicates a one-phase system.

Table 3 shows that the E^0 values decrease with increase in the cobalt content. By contrast, the cadmium content has a small effect on the E^0 values. Furthermore, the cadmium contents have a small effect on the ϕ/RT values; the ϕ/RT values tend to decrease with increase in the cobalt content as shown in Fig. 7. The decrease in ϕ/RT values makes the OCP variation approach more closely the Nernst equation curve in Eq. (6). It appears that the ϕ/RT values also affect the continuous charge–discharge characteristics, as shown in Figs. 4 and 5; the potential variation is greater in proportion with the cobalt content.

Fig. 6 shows, however, that the OCP data and the calculated data do not fit at the end of the discharge. In particular, it appears that the disagreement of the OCP data and the calculated data tend to increase with increase in cobalt content.

Table 3
E^0 and ϕ/RT values and chemical composition (Table 1) for nickel hydroxide samples

Sample	E^0 values (V)	ϕ/RT	Chemical composition	
			Co (wt.%)	Cd (wt.%)
A	0.386	2.0	0.19	$\ll 0.01$
B	0.369	1.8	2.5	$\ll 0.01$
C	0.363	1.7	4.6	$\ll 0.01$
D	0.330	1.3	9.9	$\ll 0.01$
E	0.385	1.9	0.62	3.1
F	0.383	1.8	0.73	6.4
G	0.356	1.5	5.4	3.2
H	0.327	1.3	10.2	3.2

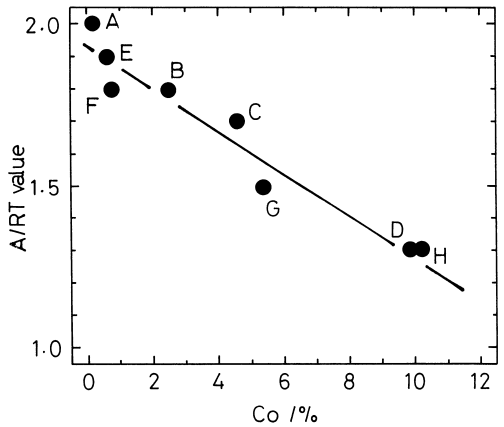

Fig. 7. Effect of cobalt content on ϕ/RT value. A: 0.19 wt.% Co; B: 2.5 wt.% Co; C: 4.6 wt.% Co; D: 9.9 wt.% Co; E: 0.62 wt.% Co, 3.1 wt.% Cd; F: 0.73 wt.% Co, 6.4 wt.% Cd; G: 5.4 wt.% Co, 3.2 wt.% Cd; H: 10.2 wt.% Co, 3.2 wt.% Cd.

Recently, quartz crystal microbalance (QCM) studies [31–34] and Raman spectroscopy [35] suggest that alkaline cations, such as K^+, Na^+, and Li^+, and water molecules can be incorporated into the nickel oxide lattice. The QCM measurements revealed an increase in the mass of a nickel electrode during charge and a decrease during discharge [31–34]. We use β-$Ni(OH)_2$ as an active material in the present study, although α-$Ni(OH)_2$ was commonly used in previous studies [31–35]. The structure of nickel hydroxide (α-$Ni(OH)_2$ and β-$Ni(OH)_2$) is very important in charge–discharge characteristics [18]. It seems, however, that the QCM data and the Raman spectroscopy data on incorporation of alkaline cations and water molecules into the nickel oxide lattice could be equally applicable in the case of β-$Ni(OH)_2$. The incorporation reaction of the alkaline cations and water molecules into the nickel oxide lattice is not assumed in Eqs. (2)–(4); the reaction of the nickel electrodes will change from a symmetrical to an asymmetrical reaction. The asymmetrical reaction in the discharge would affect the symmetrical interaction term, which was assumed to depend linearly on x in Eq. (6), and result in a difference between the OCP curve and the calculated curve at the end of the discharge.

Mo et al. [34] employed the QCM method and showed that the addition of cobalt to the nickel hydroxide lattice modifies the structural properties during the charge–discharge process. The structural properties of the nickel oxide electrode modified with the addition of cobalt may also affect the interaction term ($\epsilon_{int}(x)$). Although the OCP variation in the discharge is closely related to the cobalt content, no clear explanation can be given in the present time.

5. Conclusions

XRD measurements have shown that the d_{001} value (interlayer distance in the nickel hydroxide) decreases with

increase in cobalt content, while the d_{100} value increases with increase in cadmium content.

During the discharge process of the nickel oxide electrode, the variation in OCP follows an S-shaped curve. With one fitting parameter calculated data using thermodynamic theory and experimentally obtained OCP variations are in good agreement except at the end discharge. Moreover, the ϕ/RT and E^0 values decrease with increase in cobalt content, while the addition of cadmium has only a small effect on the ϕ/RT and E^0 values. The disagreement between the OCV data and the calculated data is manifested at the end of discharge and increases with cobalt content.

References

[1] A. Kozawa, R.A. Powers, J. Electrochem. Soc. 113 (1966) 870.
[2] A. Kozawa, R.A. Powers, Electrochemical Technology 5 (1967) 535.
[3] R.S. Crandall, P.J. Wojtowicz, B.W. Faughnan, Solid State Commun. 18 (1976) 1409.
[4] S. Atlung, T. Jacobsen, Electrochim. Acta 26 (1981) 1447.
[5] F.L. Tye, Electrochim. Acta 30 (1985) 17.
[6] R. Barnard, C.F. Randell, F.L. Tye, J. Appl. Electrochem. 10 (1980) 127.
[7] R. Barnard, C.F. Randell, F.L. Tye, J. Electroanal. Chem. 119 (1981) 17.
[8] K. Watanabe, N. Kumagai, J. Power Sources 66 (1997) 121.
[9] A.J. Berlinsky, W.G. Unruh, U.R. McKinnon, R.R. Haering, Solid State Commun. 31 (1979) 135.
[10] A.S. Nagelberg, W.L. Worrell, J. Solid St. Chem. 29 (1979) 345.
[11] A.S. Nagelberg, W.L. Worrell, J. Solid St. Chem. 38 (1981) 321.
[12] T. Jacobsen, K. West, S. Atlung, Electrochim. Acta 27 (1982) 1007.
[13] K. West, T. Jacobsen, B. Z-Christiansen, S. Atlung, Electrochim. Acta 28 (1983) 97.
[14] N. Kumagai, K. Tanno, Electrochim. Acta 36 (1991) 935.
[15] S.U. Falk, A.J. Salkind, Alkaline Storage Batteries, Wiley, New York, 1969.
[16] D.M. MacArthur, J. Electrochem. Soc. 117 (1970) 729.
[17] Z. Takehara, M. Kato, S. Yoshizawa, Electrochim. Acta 16 (1971) 833.
[18] P. Oliva, J. Leonardi, J.F. Laurent, C. Delmas, J.J. Braconnier, M. Figlarz, F. Fievet, A. de Guibert, J. Power Sources 8 (1982) 229.
[19] G.W.D. Briggs, P.R. Snodin, Electrochim. Acta 27 (1982) 565.
[20] D.F. Pickett, J.T. Maloy, J. Electrochem. Soc. 125 (1978) 1026.
[21] D.H. Fritts, J. Electrochem. Soc. 129 (1982) 118.
[22] M. Oshitani, Y. Sasaki, K. Takashima, J. Power Sources 12 (1984) 219.
[23] M. Oshitani, T. Takayama, K. Takashima, S. Tsuji, J. Appl. Electrochem. 16 (1986) 403.
[24] R.D. Armstrong, G.W.D. Briggs, E.A. Charles, J. Appl. Electrochem. 18 (1988) 215.
[25] K. Watanabe, M. Koseki, N. Kumagai, J. Power Sources 58 (1996) 23.
[26] I. Matsumoto, M. Ikeyama, T. Iwaki, H. Ogawa, Denki Kagaku 54 (1986) 159.
[27] I. Matsumoto, M. Ikeyama, T. Iwaki, Y. Umeo, H. Ogawa, Denki Kagaku 54 (1986) 164.
[28] M. Oshitani, H. Yufu, K. Takashima, S. Tsuji, Y. Matsumaru, J. Electrochem. Soc. 136 (1989) 1590.
[29] K. Watanabe, T. Kikuoka, N. Kumagai, J. Appl. Electrochem. 25 (1995) 219.
[30] B.D. Cullity, Elements of X-ray Diffraction, Addison-Wesley, Reading, MA, 1956.
[31] G.T. Cheek, W.E. O'Grady, Electrochem. Soc. Fall Meeting 259 (1990) 374, Abstract.
[32] P. Bernard, C. Gabrielli, M. Keddam, H. Takenouti, Electrochim. Acta 36 (1991) 743.
[33] S.I.C. Torresi, C. Gabrielli, A.H.L. Goff, R. Torresi, J. Electrochem. Soc. 138 (1991) 1548.
[34] Y. Mo, E. Hwang, D.A. Scherson, J. Electrochem. Soc. 143 (1996) 37.
[35] R. Kostecki, F. McLarnon, J. Electrochem. Soc. 144 (1997) 485.